

## Single-Electron Energies, Many-Electron Effects, and the Renormalized-Atom Scheme as Applied to Rare-Earth Metals

J. F. Herbst\*†

*Laboratory of Atomic and Solid State Physics, Cornell University, Ithaca, New York 14850*

and

D. N. Lowy†

*Department of Physics, State University of New York, Stony Brook, New York 11790*

and

R. E. Watson‡

*Brookhaven National Laboratory, Upton, New York 11973*

(Received 24 March 1972)

A systematic investigation of certain electronic properties of the rare-earth metals is reported. Calculations are performed within the framework of the renormalized-atom method in which Hartree-Fock free-atom solutions, with electronic configurations appropriate to the metal, are initially computed; the wave functions are then renormalized to the Wigner-Seitz sphere and used to construct  $l$ -dependent Hartree-Fock-Wigner-Seitz crystal potentials. The following results are obtained: (i) Recent spectral information together with the free-atom solutions permits us to estimate the change in neutral-atom correlation energy associated with changing the  $4f$  electron count; contrary to expectation, we find that correlation effects are more significant in a configuration with one fewer  $4f$  and one more  $5d$  electron. (ii) Band extrema and Fermi levels are placed. (iii) The positions of occupied and unoccupied  $4f$  levels are estimated in both a one-electron approach and a multielectron method taking screening and relaxation effects into account in a definite way. The one-electron approximation for the  $4f$  levels fails badly in reproducing the results of recent photoemission experiments, while the multielectron calculations are in surprisingly good accord with experiment. The effective Coulomb-interaction energy between two  $4f$  electrons at the same site, the familiar  $U$ , is reduced from the single-particle value of approximately 27 eV to about 7 eV with the inclusion of multielectron effects. (iv) Hartree-Fock values for the  $4s$ - and  $5s$ -shell exchange splittings are compared with soft-x-ray photoemission studies of the rare-earth fluorides and oxides; the calculated  $4s$  splittings are roughly twice as large as experiment while, unexpectedly, the  $5s$  results are in almost precise agreement.

### I. INTRODUCTION

#### A. Preliminary Considerations

Rare-earth elements, characterized by open  $4f$  shells which give rise to a variety of interesting electronic and magnetic properties, have received increasing attention over the past few years. Significant free-atom spectral information has been obtained quite recently, and much work has been done to elucidate metallic properties. Band structures have been calculated for several of the metals, but the position of the  $4f$  levels has remained an exacerbating problem. This paper describes calculations employing a different method for potential construction and represents an attempt to theoretically relate  $4f$ -level,  $d$ -band, and conduction-band behavior for all the rare-earth metals with the exception of Pm and Lu.

Specifically we are concerned with the difference between the Fermi energy  $\epsilon_F$  and an occupied  $4f$  level; we denote this quantity by  $\Delta_-(4f^n \rightarrow 4f^{n-1})$ . Similarly,  $\Delta_+(4f^n \rightarrow 4f^{n+1})$  represents the position

of an unoccupied  $4f$  level relative to  $\epsilon_F$ . Put another way,  $\Delta_-(4f^n \rightarrow 4f^{n-1})$  is the energy needed to excite an  $f$  level into the conduction band, while  $\Delta_+(4f^n \rightarrow 4f^{n+1})$  is the cost necessary to convert a conduction electron into a localized  $4f$  at a metallic site already having  $n$   $4f$  electrons present. We observe that the sum

$$U = \Delta_-(4f^n \rightarrow 4f^{n-1}) + \Delta_+(4f^n \rightarrow 4f^{n+1}) \quad (1.1)$$

is the energy difference between the unoccupied and occupied  $4f$  levels.  $U$  is encountered in Anderson's theory of local-moment formation and in first approximation is given by the Coulomb repulsion energy of two  $4f$  electrons at the same site.

$\Delta_-(4f^n \rightarrow 4f^{n-1})$  might nominally be identified with  $\epsilon_F - \epsilon_{4f}$ , the one-electron energy of a  $4f$  electron in the solid relative to the Fermi level. It is important to recall, however, that the  $4f$ 's are indeed localized so that the  $4f$  excitations are single-site processes. We can expect that addition or removal of an  $f$  electron may cause significant relaxation of the  $4f$  shell and its neighboring core

shells, and that screening by the conduction electrons must also be considered. From Herring's discussion<sup>1</sup> of the Hubbard model for transition metals we know that these processes can lead to as much as an order of magnitude reduction of the effective interaction, which is analogous to the quantity  $U$  considered here.

Recent photoemission experiments<sup>2</sup> have measured  $\Delta_-(4f^n - 4f^{n-1})$  for several of the rare earths, and we will find that the quantity  $\epsilon_F - \epsilon_{4f}$ , the one-electron approximation for the  $4f$  excitation, grossly overestimates experiment. The method we have used to describe the modification of  $\Delta_+$  and  $\Delta_-$  (and hence  $U$ ) by screening and relaxation effects is outlined in Sec. I B; these multielectron estimates are in good numerical agreement with the existing experimental results.

### B. Scheme

Inclusion of multielectron effects in the calculation of  $\Delta_{\pm}$  (i.e.,  $\Delta_+$  or  $\Delta_-$ ) necessitates computation of total energy differences between various configurations, a numerical problem somewhat more complicated than the calculation of one-electron eigenvalues. Our aim has been to construct a scheme which is first of all computationally viable, but which simultaneously retains at least some degree of physical realism. The method adopted is outlined below.

(i) Exploiting the single-site nature of the  $f$  excitations, we describe a rare-earth metal as a periodic array of atomic cells, each of which consequently must be electrically neutral. The renormalized-atom method of Watson, Ehrenreich, and Hodges<sup>3</sup> provides a convenient framework for such a description. The Hartree-Fock problem for the free atom is first solved, assuming the electronic configuration  $4f^n 5d^{m-1} 6s^1$  appropriate to the metal ( $m$  is the valence). The free atoms are prepared for packing in the Wigner-Seitz (WS) cell of the solid by truncating their wave functions at the WS radius  $r_{WS}$  and renormalizing them to the WS sphere;  $l$ -dependent potentials are then derived from these renormalized wave functions. Both free- and renormalized-atom total energies are calculated in order to find the change in total energy on passing from the free to renormalized atom. Since differences in energies are sought, we attempt to employ approximations for which errors in the total energy computed for the  $4f^n$  configuration will be compensated by corresponding errors in the treatment of the  $4f^{n+1}$  case.

(ii) We take advantage of free-atom spectral data to correct our Hartree-Fock estimates of  $\Delta_{\pm}$  for the change in correlation energy,  $\xi_+$  or  $\xi_-$ , associated with the alteration of free-atom  $f$  count. If  $\xi_{\pm}$  is primarily associated with the localized  $f$

electrons, its value should be appropriate to that in the metallic state. Unfortunately, the  $5d$  electrons, whose wave functions change drastically in going to the solid, also significantly influence it. We will compare differences in free-atom correlation energies obtained for the rare earths with analogous quantities calculated<sup>4</sup> for the iron series. Quite different behavior will be observed.

(iii) The renormalized-atom wave functions are used to generate  $l$ -dependent potentials of the Hartree-Fock-Wigner-Seitz<sup>3,5</sup> variety from which  $4f$ ,  $5d$ , and  $6s$  bands are deduced. This approach to potential construction allows explicit treatment of exchange effects without invoking the  $\rho^{1/3}$  approximation and includes correlation effects to the extent that an electron samples a full exchange-correlation or self-Coulomb hole centered at the cell in question. Use of this kind of potential is questionable for the  $6s$  "conduction" bands because of the delocalized character of the  $6s$  electrons in the solid, but it can be argued that it is at least as suitable as the standard local-density constructs for the  $5d$  bands. In view of the local atomic nature of the  $4f$  electrons, however, it is vital that this type of potential be employed when attempting to place the  $4f$  levels. Band results will be reported for all the rare earths but promethium, which is radioactive, and lutetium, whose  $4f$  shell is full.

(iv) Relaxation of the  $4f$  shell and the  $5s$ ,  $5p$ ,  $5d$ , and  $6s$  shells outside it as a result of changing the number of  $4f$  electrons by one is straightforwardly accounted for in our scheme by repeating the free-atom and renormalization calculations for the  $4f^{n\pm 1} 5d^{(m-1)\mp 1} 6s^1$  configurations. The associated ion potentials might then be used in a Friedel-type theory to calculate the screening of this apparent impurity by the conduction electrons in the metal. Since these materials exhibit a high  $d$ -band and virtually no  $s$ -band density of states in the vicinity of  $\epsilon_F$ , this involves screening by  $d$  electrons. We require, however, not some simple measure of the screening but the energy associated with it. This presents a formidable theoretical problem with which we are not prepared to deal directly. Instead we assume that the charge neutrality of the WS cell is preserved upon alteration of the  $4f$  count. The remainder of the lattice is taken to be fixed and  $\Delta_{\pm}$  can be identified with the change in total energy at the single site. Assuming that  $d$  screening dominates, we have chosen to describe the excited cell with a band structure appropriate to the  $4f^{n\pm 1} 5d^{(m-1)\mp 1} 6s^1$  configurations. This scheme provides a well-defined method for treating the relaxation of the  $4f$ ,  $5s$ , and  $5p$  shells but offers a less precise measure of the  $5d$ - and  $6s$ -band electron contributions to the energy shifts. Our estimate for  $\Delta_{\pm}$  becomes

$$\Delta_{\pm} \approx -\xi_{\pm} + \delta\mathcal{E} + \delta \left[ \int_{\text{band bottom}}^{\epsilon_F} \epsilon N(\epsilon) d\epsilon - \sum_i \epsilon_i \right]. \quad (1.2)$$

Here  $\xi_{\pm}$  is the correlation-energy change described previously;  $\delta\mathcal{E}$  is the difference in renormalized-atom total energies of the initial  $4f^n 5d^{m-1} 6s^1$  and final  $4f^{n+1} 5d^{(m-1)+1} 6s^1$  configurations:

$$\delta\mathcal{E} = \mathcal{E}(4f^{n+1} 5d^{(m-1)+1} 6s^1) - \mathcal{E}(4f^n 5d^{m-1} 6s^1), \quad (1.3)$$

where

$$\mathcal{E} = \sum_i \epsilon_i - (\text{double-counted two-electron terms}); \quad (1.4)$$

the  $\epsilon_i$  are the renormalized one-electron energies. The index  $i$  in Eq. (1.2) ranges only over the renormalized  $5d$  and  $6s$  states, and the term in brackets represents the change in energy resulting from replacement of the renormalized  $5d$  and  $6s$  one-electron terms by band energies appropriate to the solid. This implicitly assumes that the two-electron terms of Eq. (1.4), calculated for the renormalized atom, are identical to those in the metal. Retaining the two-electron terms as far as the renormalized-atom stage of our calculation is the limit of practicable computation. Barring some self-consistent scheme of band-potential construction it is rather difficult to provide a more satisfactory treatment of these terms. Use of the renormalized-atom estimates for the solid may introduce an error as great as 1 eV/atom in the energy of a given configuration.  $\Delta_{\pm}$ , however, is given by the difference between two such energies, and the resultant error is small, we believe, in comparison to those introduced by the other approximations. The primary uncertainty resides in attributing charge neutrality and a band structure to the single excited cell as described above. It is certainly justifiable as a practical computational scheme, and it provides at least some measure of the way in which screening and relaxation affect  $\Delta_{\pm}$ . We will find that the  $\Delta_{\pm}$  estimated in this way are in rather startling accord with the existing experimental data.

These matters are taken up in the following sections. Free-atom solutions and correlation energies are discussed in Sec. II, while Sec. III describes the renormalization procedure. Band results are given in Sec. IV, and Sec. V compares our estimates of  $\Delta_{\pm}$  with experiment. Recently exchange splittings of the  $4s$  and  $5s$  shells have been observed in rare-earth trifluorides and trioxides by means of soft-x-ray photoemission.<sup>6</sup> These data will be compared with Hartree-Fock estimates in the Appendix.

## II. FREE ATOMS

This section deals with the free-atom solutions which form the initial phase of our calculations.

Apart from the rare earths' open  $4f$  shell, the rare earths and the transition metals exhibit a similar electronic structure. The characteristic configuration for the transition-metal conduction band is normally assumed to be  $3d^{m-1} 4s^1$ , and the corresponding lanthanide configuration is here taken to be  $5d^{m-1} 6s^1$ , where, for neutral atoms,  $m$  defines the valence associated with the  $4f$  and closed-shell "core" inside. We determine free-atom eigenvalues and eigenfunctions of the  $4f^n 5d^{m-1} 6s^1$  configurations of differing  $f$ -electron count ( $n$ ), with a compensating change in conduction-electron count ( $m$ ) to preserve charge neutrality, as a starting point for estimating  $4f$  excitation energies in the solid. In the spirit of the normal paramagnetic-band description applied to most metals we treat the  $5d$  and  $6s$  shells within the average of configuration approximation<sup>7,8</sup> but, unlike the normal treatment, we require that the  $4f$  electrons be in the Hund's-rule ground- $LS$  configuration in which they are found in the free atom<sup>9</sup> and, in first approximation, in the metal.

Self-consistent Hartree-Fock results are obtained as follows for the  $4f$  shell, the closed  $5s$  and  $5p$  shells, and the open  $5d$  and  $6s$  shells which generate the conduction band in the solid. The direct and exchange potential from a fixed ion core is first constructed from the nine closed shells lying inside the  $4f$  shell, using the self-consistent  $2+$  and  $3+$  ion wave functions calculated by Freeman and Watson.<sup>10</sup> A numerical Hartree-Fock calculation is then carried out for the five outer electron shells subject to this fixed-core potential. This yields self-consistent one-electron eigenvalues and wave functions for the outer electrons.

We are interested both in one-electron energies and in the total energy difference between configurations differing in  $4f$  electron count. Given a frozen inner core common to the two configurations, the change in total energy is

$$\delta E_{\text{HF}} = \delta \left[ \sum_{\substack{i=5 \\ \text{outermost shells}}} \epsilon_i - \frac{1}{2} \sum_{i>j} U_{ij} - \delta(m_{si}, m_{sj}) J_{ij} \right]_{\text{frozen core}}, \quad (2.1)$$

where the  $\epsilon_i$  are the calculated one-electron eigenvalues,  $U_{ij}$  is the direct Coulomb integral, and  $J_{ij}$  is the exchange term; as discussed in the context of Eq. (1.4), these two-electron matrix elements must be subtracted to avoid double counting. (Note that the large parentheses contain *only* those contributions which change with changing configuration.) Use of the initial-state core for both configurations should place the final-state energy too high, and vice versa. Errors in doing this are compensated

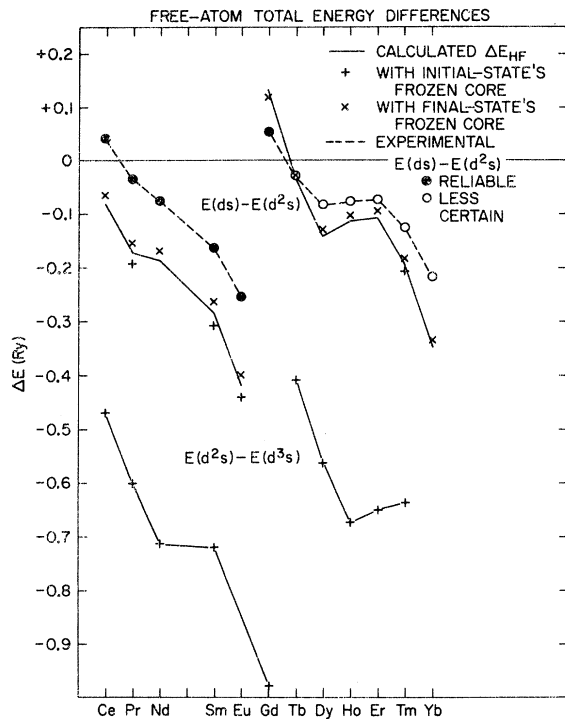


FIG. 1. Calculated and experimental estimates of the splitting between free rare-earth atom  $4f^n 5d^{m-1} 6s$  configurations of differing  $4f$  count. Hartree-Fock results are shown for  $(m=2) \rightleftharpoons (m=3)$  and  $(m=3) \rightleftharpoons (m=4)$ . The  $5d$  and  $6s$  shells are treated in the average-of-configuration (a-of-c) scheme, and the  $4f$  shell is in the Hund's-rule ground  $JLS$  state. Experimental results for  $(m=2) \rightleftharpoons (m=3)$  have been corrected to the a-of-c scheme for the  $5d$  and  $6s$  shells by the use of Slater-Condon theory and Slater integrals calculated with the Hartree-Fock wave functions. The experimental results plotted for Nd, Sm, and Gd are based on reliable data for both the  $d^2s$  and  $ds$  configurations, while those for Ce, Pr, and Eu are based on apparently trustworthy extrapolation as well as reliable data. The results for Tm and Yb employ reliable data for the  $ds$  configuration and doubtful data for the  $d^2s$ . The Tb, Dy, Ho, and Er points rely on interpolation between the Gd and Tm, Yb results for the  $d^2s$  configuration and are thus the least reliable. See Ref. 11 for the sources of experimental data.

by the fact that the core contributions do not have to be accounted for in the total energy expressions. This leads to increased computational accuracy.

The calculated curves of Fig. 1 summarize the results of this procedure. For the  $(m=2) \rightarrow (m=3)$  transition [the solid  $E(ds) - E(d^2s)$  curve in the figure] examples are given in special cases for which both initial- and final-state common cores have been used. As emphasized above, the exact result must lie between these two approximations. Satisfyingly, the two points are separated by less than 0.05 Ry. Assuming a similar spread for the  $(m=3) \rightarrow (m=4)$  transition, we place the exact Hartree-Fock result

$\approx 0.02$  Ry above the 3+ common-core points shown in Fig. 1. Further refinement of these calculations and/or inclusion of relativistic effects are inappropriate in view of the approximations made when we consider the behavior of these levels on inserting them into the metal. Note that the negative values given on the plot indicate the stability of the  $m$  configuration relative to the  $m+1$ . For example, the calculations predict that, except for Gd, the divalent ( $m=2$ ) free-atom configuration is stable relative to its trivalent ( $m=3$ ) counterpart. As shown by the experimental plot in the figure, this prediction is correct for all the atoms but Ce.

We would prefer to use experimental information to describe the free-atom  $m \rightarrow m+1$  transition, employing calculations only to describe the effects of passing from the free atom to the metal. This would enable us to account for any contribution of free-atom correlation energies, which by definition are omitted from the Hartree-Fock estimates. Unfortunately, spectral data for the rare earths are incomplete and uncertain.<sup>11</sup> The available information is collected on the experimental plot of Fig. 1. Note that the pattern displayed is similar to that calculated. As the symbols indicate, the values are well determined for the first half of the row. The uncertainty for the heavier elements is due to poor determination of the  $f^n d^2s$  ( $m=3$ ) level relative to the ground state. The values shown in Fig. 1 are established by using, where available, the separation of the lowest energy levels of the appropriate configurations. These ground  $LS$  states are shifted to an average-of-configuration<sup>7,8</sup> description for the  $5d$  and  $6s$  shells, but not the  $4f$  (which is in the ground  $JLS$  state), using Condon-Slater-Racah<sup>9</sup> theory and the unscreened Slater integrals

$$F^k(a, b) \equiv 2e^2 \int_0^\infty \int_0^\infty \frac{r^k}{r^{k+1}} P_a^2(r) P_b^2(r') r^2 dr r'^2 dr' \quad (2.2)$$

and

$$G^k(a, b) \equiv 2e^2 \int_0^\infty \int_0^\infty \frac{r^k}{r^{k+1}} P_a(r) P_b(r) P_a(r') P_b(r') \times r^2 dr r'^2 dr' \quad (2.3)$$

obtained from our calculated Hartree-Fock radial eigenfunctions  $P(r)$ .

This introduces two possible sources of error. First, we have used unscreened  $F^k$  and  $G^k$  integrals. By unscreened we mean those calculated, as opposed to the "screened" values one would obtain by fitting the observed spectra with Condon-Slater-Racah multiplet-energy expressions having  $F^k$  and  $G^k$  as adjustable parameters. From previous experience<sup>4,8</sup> the screened Slater parameters so obtained are of the order of three-fourths of the

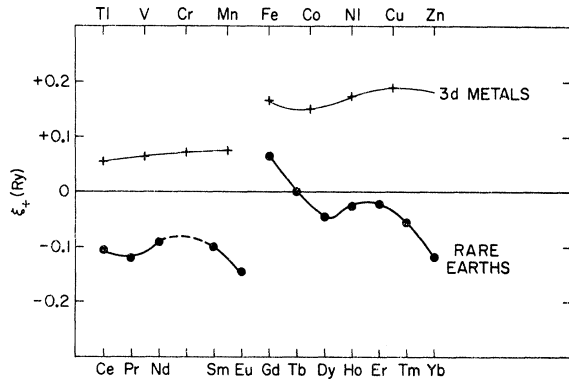


FIG. 2. Difference in correlation energy  $\xi_+$  for the  $4f^{n-1}5d6s \rightarrow 4f^n5d^26s$  free-atom transition in the rare earths and for the transition between ground multiplets of the divalent  $3d^{n+1}$  and trivalent  $3d^n$  configurations of the iron-series elements.

unscreened integrals. If such screened parameters had been used here, the experimental curve of Fig. 1 would shift upward by approximately 0.01 Ry at each end (near Ce and Yb), the shift increasing to about 0.025 Ry around the center (near Gd). Second, the energy of the lowest  $J$  level of a given  $LS$  term is always taken when using the spectral data, and spin-orbit effects involving the  $4f$ ,  $5d$ , and  $6s$  shells contribute to the level position. To investigate the impact of this unwanted contribution, the energy of the lowest state was compared with the center of gravity of the set of  $J$  levels belonging to the  $LS$  multiplet in the few cases for which sufficient data exist. With the possible exception of Eu the experimental points of Fig. 1 are affected by less than 0.01 Ry in the cases tested. This estimate averages out the spin-orbit effects of the  $4f$  shell as well, something we do not necessarily desire, and thus overestimates the error.

Figure 2 displays the correlation-energy difference  $\xi_+$  associated with the  $(m=3) \rightarrow (m=2)$  transition.  $\xi_+$  is the difference between the observed spectral energy shift and the calculated Hartree-Fock energy shift for a transition. We define it here as

$$\begin{aligned} \xi_+ &= [E(d^2S) - E(ds)]_{\text{expt}} - [E(d^2s) - E(ds)]_{\text{HF}} \\ &= [E(d^2s)_{\text{expt}} - E(d^2s)_{\text{HF}}] - [E(ds)_{\text{expt}} - E(ds)_{\text{HF}}] \\ &\equiv E_{\text{corr}}(f^n d^2s) - E_{\text{corr}}(f^{n+1} ds). \end{aligned} \quad (2.4)$$

Since the Hartree-Fock calculation is a variational estimate, the correlation energies  $E_{\text{corr}}$  are always nonpositive, so that  $\xi_+ < 0$  means that the correlation is greater in the  $f^n d^2s$  configuration. Also plotted in Fig. 2 is a similar quantity involving the ionization energy necessary to raise the divalent  $3d^n$  transition-metal ions to their trivalent

$3d^{n-1}$  states<sup>4</sup>:

$$\xi_+ \equiv E_{\text{corr}}^{2+}(3d^n) - E_{\text{corr}}^{3+}(3d^{n+1}). \quad (2.5)$$

In Eq. (2.4) the  $f$  electrons are in the ground multiplet for both the initial and final configurations, and similarly for the  $d$ -electron configurations of Eq. (2.5). In the latter case, however, charge neutrality has not been maintained. Both  $\xi_+$  curves are characterized by a jump at the point where the  $f$  or  $d$  shell becomes over half-filled, i. e., when the ionized  $3d$  or  $4f$  electron is of minority spin. Such an electron has no exchange terms and presumably suffers strong correlation effects with the majority of the shell.

The transition metals exhibit the expected behavior in that the magnitude of the correlation energy is greater in the  $d^{n+1}$  than in the  $d^n$  configuration ( $\xi_+ > 0$ ). For the rare earths, on the other hand, the negative  $\xi_+$  plotted for all but Gd and Tb indicate that correlation effects are stronger in the state having one fewer  $4f$  and one more  $5d$  electron. This is quite surprising. We have no reason not to believe this to be a real trend and not an artifact caused by computational errors or by the experimental data as used.

We also require the quantity

$$\xi_- = E_{\text{corr}}(f^n d^2s) - E_{\text{corr}}(f^{n-1} d^3s) \quad (2.6)$$

associated with the  $(m=3) \rightarrow (m=4)$  transition. Lacking any experimental data whatsoever we make the drastic assumption that the  $\xi_+$  can be used for this purpose; that is, we assume

$$\xi_-(f^n \rightarrow f^{n-1}) = \xi_+(f^{n-1} \rightarrow f^n). \quad (2.7)$$

This  $\xi_-$  is then used to determine the "experimental" values for the  $(m=3) \rightarrow (m=4)$  transition plotted in Fig. 3. These experimental values will be used in subsequent sections. This assumption of common correlation effects is obviously poor, but suffices for our purposes.

### III. RENORMALIZATION

In this section we pass from the free-atom results to the description of an "atom" characteristic of the metal; this is accomplished by means of the renormalized-atom method. Wave functions in this description are obtained by truncating the free-atom radial wave functions at  $r_{\text{WS}}$  and multiplying by constants chosen to renormalize them to the WS sphere. Values of  $r_{\text{WS}}$  computed from the lattice constants are given in Table I. We see that the trivalent elements display the famous lanthanide contraction,  $r_{\text{WS}}$  decreasing with increasing atomic number. Construction of the Hartree-Fock potentials proceeds exactly as in the free-atom case but employs the renormalized wave functions:

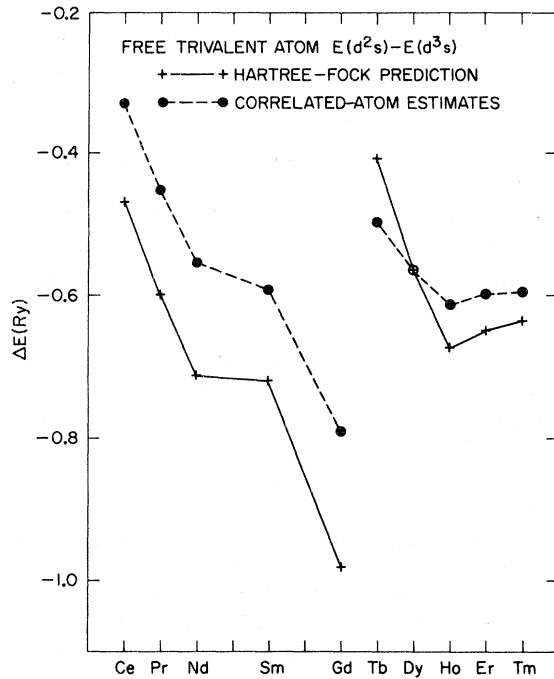


FIG. 3. Free-trivalent-atom splittings between the  $4f^n 5d^2 6s$  and  $4f^{n-1} 5d^3 6s$  configurations. The solid curve represents Hartree-Fock estimates, while the dashed curve is generated by correcting Hartree-Fock theory for correlation effects by assuming the divalent atom ( $4f^{n-1} 5d 6s \rightarrow 4f^n 5d^2 6s$ ) correlation contributions obtainable from Fig. 1.

$$\begin{aligned}
 V_i(r) = & -\frac{2z}{r} + 2 \sum_j \int_{\text{WS sphere}} |\phi_j(\vec{r}')|^2 \frac{d\vec{r}'}{|\vec{r} - \vec{r}'|} \\
 & - 2 \sum_j \delta(m_{sj}, m_{st}) \frac{\phi_j(\vec{r})}{\phi_i(\vec{r})} \\
 & \times \int_{\text{WS sphere}} \phi_j^*(\vec{r}') \phi_i(\vec{r}') \frac{d\vec{r}'}{|\vec{r} - \vec{r}'|}. \quad (3.1)
 \end{aligned}$$

In this expression  $\phi_i(\vec{r})$  is a renormalized electron wave function, and the sums extend over all occupied states. When required, renormalized electron energies are simply evaluated<sup>12</sup> as

$$\epsilon_i = \langle \phi_i | -\nabla^2 + V_i | \phi_i \rangle. \quad (3.2)$$

Only the  $5d$  and  $6s$  wave functions experience any significant renormalization. As much as 80% of the  $6s$  charge and 40% of the  $5d$  charge is brought inside  $r_{\text{WS}}$ , while the corresponding amount is no more than 1% for the  $5p$  and 0.4% for the  $4f$  and  $5s$  shells. Core-electron wave functions are negligible in the neighborhood of  $r_{\text{WS}}$  and consequently remain unchanged during the renormalization process. Table II summarizes charge-transfer infor-

TABLE I. Crystal structure and Wigner-Seitz radii of the rare-earth metals.

Element	Number of $4f$ electrons	Crystal structure	$r_{\text{WS}}$ (a.u.)
$\gamma$ -Ce	1	fcc	3.81
Pr	2	dhcp	3.82
Nd	3	dhcp	3.80
Pm		omitted	
Sm	5	rhomb	3.76
Eu	7	bcc	4.26
Gd	7	hcp	3.76
Tb	8	hcp	3.71
Dy	9	hcp	3.70
Ho	10	hcp	3.68
Er	11	hcp	3.67
Tm	12	hcp	3.65
Yb	14	fcc	4.03

mation for the trivalent and divalent elements according to valence-electron configuration. It can be seen that the effect of renormalization becomes less severe as the number of  $f$  electrons is decreased. This is simply because the shielding of the nuclear potential by the  $f$ 's becomes less effective as their number decreases so that the outer electrons are more strongly bound; as a result, more of their free-atom charge resides within  $r_{\text{WS}}$ . Divalent Eu and Yb have the largest ion cores and WS radii, and we see that their charge shifts are somewhat smaller than those in the corresponding trivalent-element configurations.

Figure 4 displays the free and renormalized  $4f$  one-electron energies.  $\epsilon_{4f}$ , the renormalized value, is shifted upward relative to the free-atom result by approximately 0.5 Ry. The magnitude of this shift depends largely on the size of  $r_{\text{WS}}$ ; Eu and Yb, with significantly greater values of  $r_{\text{WS}}$ , exhibit smaller increases of 0.3–0.4 Ry. The binding increases from cerium to gadolinium and stabilizes thereafter in the row (except for obvious deviations at the divalent elements). Behavior of this kind has also been observed for the  $d$  electrons of the transition metals.<sup>3</sup>

Use of the renormalized-atom potential causes the  $\epsilon_{4f}$  points of Fig. 4 to lie somewhat higher than a self-consistent band-potential scheme would pre-

TABLE II. Percentage of charge transferred inside  $r_{\text{WS}}$  on renormalization of free-atom wave functions.

	Configuration	$4f$	$5s$	$5p$	$5d$	$6s$
Trivalent elements	$f^{n+1} d s$	0–0.4	0–0.2	0.4–1.2	30–40	70–80
	$f^n d^2 s$	0–0.1	0–0.2	0.3–0.8	20	70–80
	$f^{n-1} d^2 s$	0–0.1	0–0.1	0.2–0.6	15	65–75
Divalent elements (Eu and Yb)	$f^n d s$	0.0	0.0	0.1–0.2	25–35	60–65
	$f^{n-1} d^2 s$	0.0	0.0	0.1	15	55–60

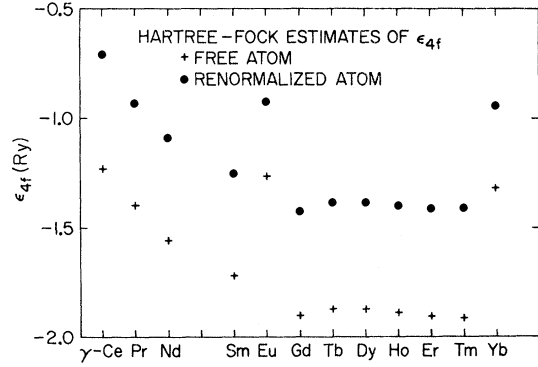


FIG. 4. Free- and renormalized-atom estimates of  $\epsilon_{4f}$  for the rare earths. The configuration is the trivalent  $4f^n 5d^2 6s$  except for Eu and Yb, which are in the divalent  $4f^{n-1} 5d 6s$ .

dict. This is because the  $5d$  wave function at the bottom of the band is less diffuse in the renormalized picture, which makes the potential more repulsive and raises the one-electron energies with respect to the vacuum level. What ultimately interests us, however, is not the position of  $\epsilon_{4f}$  relative to vacuum but with respect to the  $d$  bands and the Fermi level in them. We anticipate that  $\epsilon_{4f}$  may still lie slightly high; that is,  $\epsilon_F - \epsilon_{4f}$  may be lower than a self-consistent procedure would indicate.

Although the  $4f$  one-electron energy shifts are sizable, they will result in estimates of  $\Delta_-(4f^n - 4f^{n-1})$  in Sec. V which are not in satisfactory agreement with the present experimental findings. This is presumably because  $\epsilon_{4f}$  is the excitation energy of a  $4f$  electron without allowing for the relaxation of the remaining states to the final configuration.

We turn therefore to estimating total energy differences for various excitations. Since only the outermost wave functions are altered, we may write the total energy  $E_{\text{tot}}$  as

$$E_{\text{tot}} = \mathcal{E} + \text{const}, \quad (3.3)$$

where the constant denotes those terms arising from the kinetic and nuclear potential energy of and the electron-electron terms among the  $1s^2 2s^2 \dots 4p^6 4d^{10}$  inner-core states. Since these states remain fixed in the computations, these terms make no contribution to the  $\Delta_{\pm}$  of Eq. (1.2).  $\mathcal{E}$  is that part of the energy which is affected by changes in the outer wave functions and is given by

$$\mathcal{E} = \sum_i \epsilon_i - \frac{1}{2} \sum_{i>j} [U_{ij} - \delta(m_{si}, m_{sj})J_{ij}]. \quad (3.4)$$

This term appeared inside the large parentheses of Eq. (2.1). It is easy to demonstrate that this can be rewritten

$$\mathcal{E} = \frac{1}{2} \sum_{i=4f, \dots, 6s} [\epsilon_i + \langle \phi_i | -\nabla^2 + V_{\text{core}} | \phi_i \rangle], \quad (3.5)$$

where  $V_{\text{core}}$  is the core potential acting on the electron in state  $i$  and arising from the nucleus and inner-core electrons; this form facilitates computation of  $\mathcal{E}$ .

The total energy change  $\eta$  due to renormalization is given by

$$\eta = \mathcal{E}^{\text{ren}} - \mathcal{E}^{\text{free}}, \quad (3.6)$$

where  $\mathcal{E}^{\text{ren}}$  is expression (3.5) evaluated<sup>13</sup> with the renormalized wave functions and  $\mathcal{E}^{\text{free}}$  that with the corresponding free-atom states. Results are obtained for  $m = 2, 3, 4$  for the trivalent elements and  $m = 2, 3$  for divalent Eu and Yb.  $\eta$  can be as large as 0.2 Ry but differences of the sort  $\eta(m) - \eta(m \pm 1)$  are of interest in evaluating  $\Delta_{\pm}$ , and these differences are never larger than about 0.02 Ry, hence insignificant.  $\mathcal{E}^{\text{ren}}$  does not offer an adequate description of a cell in the metal because band effects have not yet been taken into consideration. To this point we have correctly accounted for changes in the two-electron energy terms encountered in Eqs. (1.4) and (3.4).<sup>13</sup>

#### IV. BAND-STRUCTURE CONSIDERATIONS AND RESULTS $\Delta_{\pm}$ AND $U$

To describe a cell in the metal we extend the renormalized-atom results of Sec. III by taking band structure into account. Determining band features for both the initial and excited cells enables us to estimate  $\Delta_{\pm}$  and  $U$  through Eqs. (1.1) and (1.2) and to contrast these values with their one-electron analogs. Our final estimates of  $\Delta_-(4f^n - 4f^{n-1})$  will be compared with experiment in Sec. V.

##### A. Placement of Bands

Information regarding rare-earth band structure is itself interesting and useful, in addition to its specific need here in estimating band contributions to  $\Delta_{\pm}$ , given the renormalized-atom starting point. The renormalized-atom potential of appropriate  $l$  is used in the radial Schrödinger equation which is solved for different choices of the energy  $\epsilon$ . We use the WS conditions at  $r_{\text{WS}}$  to establish  $4f$ ,  $5d$ , and  $6s$  band extrema. The bottom of a band is specified by that energy for which the wave function has zero derivative at  $r_{\text{WS}}$ , and the value of  $\epsilon$  for which the wave function is noded at  $r_{\text{WS}}$  determines the top of a band. These criteria were found to accurately place band extrema in the  $3d$  and  $4d$  metals.<sup>3</sup>

Fermi levels are estimated with the aid of existing band-structure computations having density-of-states curves amenable to accurate graphical integration [we need to evaluate the first term in

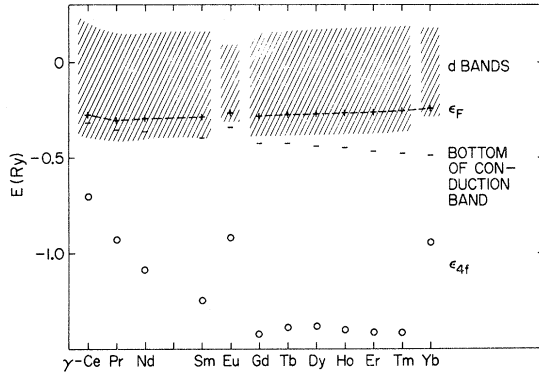


FIG. 5. Rare-earth-metal band structures predicted with  $l$ -dependent renormalized-atom potentials for atoms in their ground configurations (i.e., except for divalent Eu and Yb the configuration is the trivalent  $4f^n 5d 6s$ ). Shown are the position of the  $4f$  level,  $\epsilon_{4f}$ ; the extent of the  $d$  band; the bottom of the conduction band; and the Fermi level  $\epsilon_F$ . The vacuum zero is at the zero of the plot.

brackets in Eq. (1.2)]. With this in mind we have chosen to use augmented-plane-wave (APW) results of Freeman<sup>14</sup> for bcc europium, the relativistic calculations of Jackson<sup>15</sup> for hcp terbium in the case of the hcp metals, and the gold relativistic-APW (RAPW) calculations by Christensen<sup>16</sup> for fcc Ce and Yb. The Fermi level is placed by assuming its position relative to our  $d$ -band extrema is the same as in the full band-structure calculation; that is, we write

$$\epsilon_F = \epsilon(d \text{ bottom}) + \alpha[\epsilon(d \text{ top}) - \epsilon(d \text{ bottom})], \quad (4.1)$$

where the top and bottom of the  $d$  bands are determined as described in the preceding paragraph, and  $\alpha$  is obtained by noting the position of  $\epsilon_F$  relative to the  $d$ -band extrema in the band calculations.<sup>17</sup>

Figure 5 indicates the  $s$ -band minimum ( $\epsilon_{\Gamma_1}$ ), the top and bottom of the  $d$  bands,  $\epsilon_{4f}$ , and  $\epsilon_F$ . These energies are positioned relative to the vacuum zero, as is easily done with the renormalized-atom potentials.  $\epsilon(d \text{ bottom})$  slowly rises across the row while  $\epsilon_{\Gamma_1}$  progressively decreases. The  $d$  bandwidth decreases from Ce to Gd and remains roughly constant from Tb onwards. As a matter of record the calculated  $4f$  bandwidths are 0.03 Ry for  $\gamma$ -Ce, 0.01 Ry for Pr and Nd, and thereafter in the row never exceed 0.005 Ry. We note these even though the band description is, of course, useless for the  $4f$  electrons.

The  $d$  bands lie somewhat lower relative to  $\epsilon_{\Gamma_1}$  than in the conventional band-structure results. For example,  $\epsilon_{\Gamma_1}$  in Jackson's calculation is located 0.22 Ry below the  $d$  minimum as opposed to the 0.04-Ry value we obtain. This disparity arises

from the use of different potential constructs and different starting atomic configurations. The renormalized-atom type of potential centers the correlation hole in the WS cell in contrast with the local-density approach<sup>18</sup> in which the hole is centered at the electron's position. The latter is probably more desirable for analyzing conduction-band properties, but we feel that the potentials employed here are superior to the standard local-density constructs for the  $5d$  and especially for the highly localized  $4f$  electrons.

In order to compute the first quantity in the brackets of Eq. (1.2) we numerically integrate the density of states to find the average energy of each electron in the bands; its position relative to the  $d$  bands is noted and used to place that quantity in our calculations. As before, the full band-structure results are simply accorded to fit our  $d$  band extrema, and the average energies of interest correspondingly located. Some error is introduced by this procedure since the relative position of our  $s$  and  $d$  bands is not the same as in the conventional band results. Nevertheless, this discrepancy will not have any severe impact on the estimate of  $\Delta_{\pm}$  because that involves the difference between two average energies, both of which are subject to an error of similar sign and magnitude.

#### B. Results for $\Delta_+$ and $\Delta_-$

$\Delta_{\pm}$  represents the difference between two multielectron energies and not a simple one-electron energy, but it is clear from the way our calculations have been performed that  $\Delta_+(4f^n - 4f^{n+1})$  can be interpreted as the position of an unoccupied  $f$  level above  $\epsilon_F$  and  $\Delta_-(4f^n - 4f^{n+1})$  as the location of an occupied  $f$  level below  $\epsilon_F$ . The results are so displayed in Fig. 6. Equation (1.2) has been used for  $\Delta_{\pm}$ .  $\Delta_+(4f^n - 4f^{n+1})$  was not computed for divalent Eu and Yb, and their  $\Delta_-$  have been connected to the  $\Delta_+$  curve of the other elements because these *also* involve  $(m=2) \rightarrow (m=3)$  transitions. The breaks in the  $\Delta_{\pm}$  curves reflect the stability of the half-filled  $4f$  shell.  $\epsilon_{4f}$  is indicated in the figure, and it is evident that  $\Delta_-(4f^n - 4f^{n+1})$  is significantly smaller than  $\epsilon_F - \epsilon_{4f}$ . Screening and relaxation effects, insofar as we have incorporated them, serve to raise the energy of the occupied  $f$  levels relative to  $\epsilon_F$ , as anticipated in Sec. I. Divalent-trivalent phase transitions of rare-earth compounds are known to exist in the vicinity of Sm and Eu, and it is encouraging that the point ( $\times$ ) for Sm in Fig. 6 is just above  $\epsilon_F$  while the ( $\bullet$ ) for Eu lies just below; similar observations apply in the region of Tm and Yb, where a crossover again occurs. Our results predict unoccupied  $4f$  levels lying just above  $\epsilon_F$  for most of the rare-earth metals.

We may crudely judge the error in our calcula-

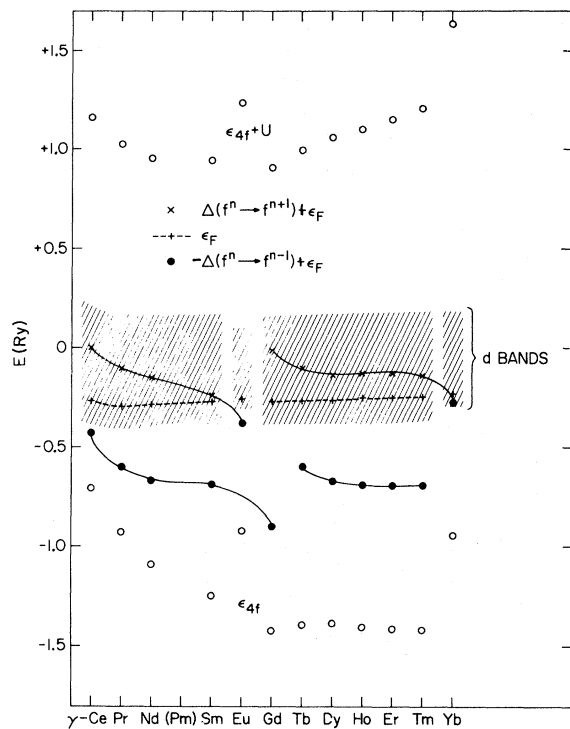


FIG. 6. One-electron and multielectron predictions of  $\Delta_+$  ( $4f^n \rightarrow 4f^{n+1}$ ) and  $\Delta_-$  ( $4f^n \rightarrow 4f^{n-1}$ ) plotted with respect to the  $d$  bands and Fermi levels of the rare earths. The one-electron estimates of  $\Delta_-$  ( $4f^n \rightarrow 4f^{n-1}$ ) are the one-electron energies  $\epsilon_{4f}$ ; the single-particle predictions for  $\Delta_+$  ( $4f^n \rightarrow 4f^{n+1}$ ) are taken to be  $\epsilon_{4f} + U$ , where  $U$  is approximated by the  $F^0(4f, 4f)$  Slater integral. The multielectron  $\Delta_+$  are plotted relative to  $\epsilon_F$  as effective one-electron energies.

tions of  $\Delta_{\pm}$  as follows.  $\gamma$ -Ce undergoes a phase transition at 95°K under normal pressure to the  $\alpha$  phase (fcc but having a smaller lattice constant), and this is thought<sup>19</sup> to be caused by the emptying of the  $4f$  shell into the conduction band. Since we predict 0.15 Ry for the  $\Delta_-$  of  $\gamma$ -Ce, we estimate that our results are in error by at most +0.15 Ry. Calculations were also performed for  $\alpha$ -Ce assuming complete absence of  $4f$  electrons and using the proper  $r_{ws}$ . It was found that the  $\alpha$  configuration was energetically more favorable than the  $\gamma$  by several hundredths of a rydberg, a difference which is in the correct direction and approaches, albeit at some distance, the energy scale corresponding to the phase transition.

The above results incorporate the free-atom correlation contribution  $\xi_{\pm}$ . Hartree-Fock estimates, simply obtained by omitting  $\xi_{\pm}$ , would lower the  $\Delta_{\pm}$  curves by approximately 0.1 Ry between Ce and Eu with smaller shifts for the heavier metals. We note that the  $\Delta_+$  curve involves the experimentally determined free atom  $\xi_+$ , whereas the  $\Delta_-$  curve incorporates the rather poor extrap-

olation given by Eq. (2.6) and Fig. 2 (see Sec. II).

### C. Parameter $U$

Finally, we turn to the estimate of  $U$ , the energy separation of the unoccupied and occupied  $4f$  levels. In the simple unscreened single-particle picture  $U$  is given by Slater integrals:

$$U_{\text{sing}} = F^0(4f, 4f) + (F^2 \text{ and } F^4 \text{ contributions}) \\ \sim F^0(4f, 4f) \sim 2 \text{ Ry} . \quad (4.2)$$

This is plotted in Fig. 6 relative to  $\epsilon_{4f}$ ; single-particle arguments predict the  $f$  holes to lie some 15 eV above the Fermi level. On the other hand, our calculation of the  $4f$  excitation energies  $\Delta_{\pm}$ , with the inclusion of screening and relaxation effects, gives the effective multielectron value

$$U_{\text{eff}} = \Delta_-(4f^n \rightarrow 4f^{n-1}) + \Delta_+(4f^n \rightarrow 4f^{n+1}) \sim 0.5 \text{ Ry} . \quad (4.3)$$

This quantity is fairly constant across the row, as Fig. 6 shows. The single-particle prediction is decreased by a factor of roughly 4. While substantial, the effect of screening is somewhat less than that obtained by Herring<sup>1</sup> for the Hubbard-model

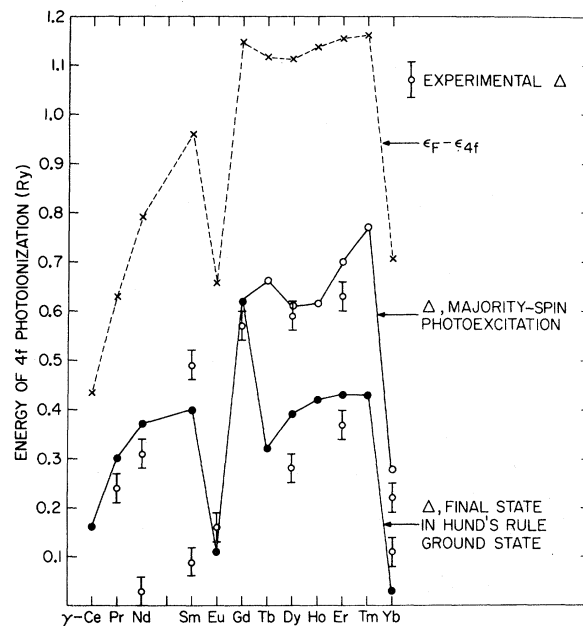


FIG. 7. Theoretical and experimental values for the photoexcitation of  $4f$  electrons in the rare-earth metals. Three sets of theoretical values are shown: (a) one-electron predictions  $\epsilon_F - \epsilon_{4f}$ ; (b) multielectron predictions for which the  $4f$ -shell final state is the Hund's-rule ground multiplet for the atoms with over half-filled  $4f$  shells (corresponding to the photoexcitation of a minority-spin  $4f$  electron); and (c) multielectron predictions for the over half-filled  $4f$ -shell atoms corresponding to photoexcitation of a majority-spin  $4f$  electron with the final state having proper  $J$ ,  $L$ , and  $S$  ( $S = S_{\text{initial}} - \frac{1}{2}$ ).

$U$  as applied to the  $3d$  transition metals, although the single-particle values  $U_{\text{sing}}$  are about the same in both instances. Perhaps these contrasting results are linked to the different character of the  $4f$  and  $3d$  electrons: The  $3d$ 's are described rather well in first approximation by band theory, whereas the  $4f$ 's are highly localized and principally atomic in nature.

### V. $4f$ -SHELL PHOTOEMISSION

Results of x-ray photoemission experiments<sup>2</sup> on rare-earth  $4f$  levels are shown in Fig. 7 together with our predictions. The one-electron  $\epsilon_F - \epsilon_{4f}$  values are shown and, as noted previously, greatly exceed the experimental findings. The shaded circles represent the estimates of  $\Delta(4f^n \sim 4f^{n-1})$  based on using Hund's-rule ground multiplets for the  $4f$  shell in both the initial and final states. These were also plotted in Fig. 6 (the shaded circles) and correspond to exciting a majority-spin electron if the  $4f$  shell is less than half-filled ( $S_{\text{final}} = S_{\text{initial}} - \frac{1}{2}$ ) and a minority spin if it is more than half-filled ( $S_{\text{final}} = S_{\text{initial}} + \frac{1}{2}$ ). Of equal interest in the latter instance, however, is the possibility of exciting a majority spin ( $S_{\text{final}} = S_{\text{initial}} - \frac{1}{2}$ ). To estimate this, a perturbation calculation was carried out employing Slater-Condon<sup>8</sup> multiplet theory. The final state was assumed to have spin  $S - 1$ , where  $S$  is the spin of the Hund's-rule ground state of the configuration, and maximum possible  $L$ ; it is thus the lowest  $JLS$  multiplet of the desired spin. Hartree-Fock  $F^k(4f, 4f)$  integrals (calculated for the final-state configuration) were used, but were scaled by a factor of 0.75 to crudely take correlation effects into account (see Sec. II). The results are given by the open circles of Fig. 7.

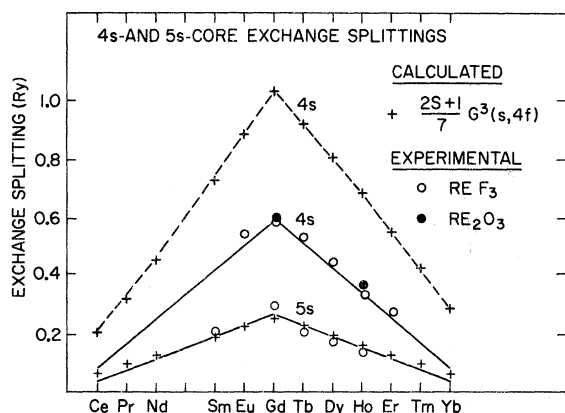


FIG. 8. Rare-earth  $4s$ - and  $5s$ -core exchange splittings as deduced from soft-x-ray photoemission experiments on rare-earth oxides and fluorides and as calculated with Slater  $G^3(ns, 4f)$  integrals obtained with ground-state (i. e., filled- $s$ -shell) trivalent-core wave functions.  $S$  is the  $4f$ -shell spin quantum number.

They represent the low-energy edge of a set of possible majority-spin photoexcitations.

Neglecting the lower-energy peaks reported for Nd and Sm, there is extraordinary agreement between theory and experiment granting the shortcomings of the theory and the uncertainties in experiment. We observe that the one-electron predictions compare quite poorly with experiment. Note also, as discussed earlier in regard to Fig. 4 (Sec. III), that the renormalized-atom scheme used here has, if anything, shifted the  $\epsilon_F - \epsilon_{4f}$  curve down too far. We thus conclude that the  $\epsilon_{4f}$  provide an inadequate description of  $f$  excitations, in contrast to experience with  $s$ ,  $p$ , and  $d$  bands in metals, and that multielectron screening and relaxation effects are significant.

### ACKNOWLEDGMENTS

We gratefully acknowledge discussions with R. L. Cohen and G. K. Wertheim and appreciate the early enthusiasm of S. Hagstrum, L. Hedin, and B. I. Lundqvist. One of us (J. F. H.) especially thanks J. W. Wilkins for penetrating conversations and persistent encouragement.

### APPENDIX: $S$ -SHELL EXCHANGE SPLITTINGS IN INSULATORS

Excitations of rare-earth  $4s$ - and  $5s$ -core levels have been observed by soft-x-ray photoemission<sup>6</sup> in some of the fluorides and oxides. Doublet structures are seen, and these have been attributed to an exchange splitting of the remaining  $s$ -shell electron in the  $4f$  exchange field. An  $s$  electron will couple to an open  $4f$  shell of some  $L$  and  $S$  to generate states with the same  $L$  and  $S \pm \frac{1}{2}$ . The intensities of the two members of the experimentally observed doublets differ in a way consistent with the different degeneracies of the  $S + \frac{1}{2}$  and  $S - \frac{1}{2}$  states. Assuming fixed radial functions, the energy splitting  $\delta E$  is given by<sup>8</sup>

$$\delta E = \frac{1}{7} (2S + 1) G^3(ns, 4f). \quad (\text{A1})$$

Values of these splittings have been estimated through use of the  $G^3$  integrals obtained in the course of our calculations for the trivalent atoms. These are compared with the experimental data in Fig. 8. The  $4s$  splittings are larger than the  $5s$  because of greater overlap with the  $4f$  shell. The  $4s$  results are rather typical of most experience in comparing computed Slater integrals with parameters obtained by fitting spectra.<sup>4,8</sup> The calculated quantities are larger, the experimental parameters having been reduced from the bare integral values by correlation and relaxation effects. Most previous experience stems from fits of spectra involving open outer valence shells of atoms, and it is interesting that similar behavior apparently occurs for the exchange splitting of an interior-

core  $s$  shell. What is beyond normal experience is the almost perfect numerical agreement for the  $5s$ -shell splittings. Along with the  $5p$ , the  $5s$  shell is outermost in the rare-earth ions of the fluorides and oxides and, therefore, at least slightly involved in covalent and overlap effects. Whether this is a factor contributing to the observed trends is unknown. These results were obtained nonrelativistically and with neutral-atom

wave functions, but the presence of the  $5d$  and  $6s$  electrons is expected to affect the  $G^3$  values by no more than 5%. More important, perhaps, is the fact that we used initial-state functions in which the  $s$  shell in question is filled. Calculations for the  $L, S \pm \frac{1}{2}$  states, with a hole in the  $s$  shell of interest, would be expected to show a mild increase in the theoretical  $5s$  splitting, causing it to lie at least slightly above experiment.

\*Research supported in part by the National Science Foundation through Grant No. GP-27355; Cornell University Graduate Fellow.

†Part of work done while Guest of Brookhaven National Laboratory.

‡Work supported by U. S. Atomic Energy Commission.

<sup>1</sup>C. Herring, *Magnetism*, Vol. IV, edited by G. T. Rado and H. Suhl (Academic, New York, 1966), Chap. IX.

<sup>2</sup>P. O. Hedén, H. Löfgren, and S. B. M. Hagström, *Phys. Rev. Letters* **26**, 432 (1971).

<sup>3</sup>R. E. Watson, H. Ehrenreich, and L. Hodges, *Phys. Rev. Letters* **24**, 829 (1970); L. Hodges, R. E. Watson, and H. Ehrenreich, *Phys. Rev. B* **5**, 3953 (1972).

<sup>4</sup>R. E. Watson, *Phys. Rev.* **118**, 1036 (1960).

<sup>5</sup>M. Chodorow, *Phys. Rev.* **55**, 675 (1939); Ph. D. thesis (Massachusetts Institute of Technology, 1939) (unpublished).

<sup>6</sup>R. L. Cohen, G. K. Wertheim, A. Rosencwaig, and H. J. Guggenheim, *Phys. Rev. B* **5**, 1037 (1972); and unpublished.

<sup>7</sup>G. H. Shortley, *Phys. Rev.* **50**, 1072 (1936).

<sup>8</sup>J. C. Slater, *Quantum Theory of Atomic Structure*, Vols. I and II (McGraw-Hill, New York, 1960).

<sup>9</sup>J. H. Van Vleck, *Theory of Electric and Magnetic Susceptibilities* (Oxford U. P., Oxford, England, 1959). We shall neglect deviations from this ground state of the kind discussed by Van Vleck for Eu.

<sup>10</sup>A. J. Freeman and R. E. Watson, *Phys. Rev.* **127**, 2058 (1962).

<sup>11</sup>The experimental optical data on which the free-atom  $4f^n 5d^2 6s - 4f^{n+1} 5d 6s$  energy splittings are based are listed by element below. The number in brackets designates the valence  $m$  of the  $4f^n 5d^{m-1} 6s^1$  configuration. For Dy and Er data exist for the  $4f^n 5d 6s^2$  and  $4f^{n+1} 6s^2$  configurations but not for the configurations of interest. These data are nevertheless vital to the placement of the trivalent ( $m=3$ ) configuration relative to the divalent ( $m=2$ ). The Tm(3) and La(3) attributions are somewhat uncertain, hence the question marks. The energy splittings we obtain are in over-all agreement with those given by L. Brewer [*J. Opt. Soc. Am.* **61**, 1101 (1971)] except in the vicinity of Sm and Eu.

La (3) J. Stein, *J. Opt. Soc. Am.* **57**, 333 (1967).

La (3?) P. F. A. Klinkenberg, *Physica* **21**, 53 (1954).

Ce (3) W. C. Martin, *J. Opt. Soc. Am.* **53**, 1047 (1963); W. J. Childs and L. S. Goodman, *Phys. Rev. A* **1**, 1290 (1970).

Nd (2,3) J. Blaise, J. Chevillard, J. Vergès, and J. F. Wyatt, *Spectrochim. Acta* **25B**, 333 (1970).

Sm (2,3) J. Blaise, C. Morillon, M. G. Schweighofer, and J. L. Vergès, *Spectrochim.*

*Acta* **24B**, 405 (1969).

Eu (2,3) H. N. Russell and A. S. King, *Astrophys. J.* **90**, 155 (1939); G. Smith and B. G. Wybourne, *J. Opt. Soc. Am.* **55**, 121 (1965); G. Smith and M. Wilson, *ibid.* **60**, 1527 (1970).

Gd (2,3) H. N. Russell, *ibid.* **40**, 550 (1950).

Gd (3) J. Blaise, J. F. Wyatt, and T. A. M. van Kleef, *Compt. Rend.* **B270**, 261 (1970).

Gd (2) T. A. M. van Kleef, R. Slooten, J. Blaise, and P. Camus, *Compt. Rend.* **B270**, 204 (1970).

Tb (3) P. F. A. Klinkenberg and E. Meinders, *Physica* **42**, 213 (1969).

Dy ( $f^9 d s_2$ ,  $f^{10} s_2$ ) J. Conway and E. F. Worden, *J. Opt. Soc. Am.* **58**, 1564 (1968); W. J. Childs, *Phys. Rev. A* **2**, 1692 (1970).

Er ( $f^{10} d s_2$ ,  $f^{11} s_2$ ) G. Racah, Z. B. Goldschmidt, and S. Toaff, *J. Opt. Soc. Am.* **56**, 407 (1966).

Tm (2) P. Camus, G. Guelachiili, and J. Vergès, *Spectrochim. Acta* **24B**, 373 (1969).

Tm (3?) P. Camus, *J. Phys. (Paris)* **27**, 717 (1966).

Yb (2) S. Nir, *J. Opt. Soc. Am.* **60**, 354 (1970).

<sup>12</sup>The first term in this matrix element is in practice calculated by truncating the free-atom kinetic-energy integral at  $r_{WS}$  rather than by differentiating the discontinuous renormalized wave function, which is zero outside  $r_{WS}$ ; the latter procedure would introduce spurious contributions to the kinetic energy.

<sup>13</sup>Use of  $\epsilon_{6s}$  in calculating  $G^{3m}$  makes our specification of the renormalized atom somewhat different than that of Ref. 3, where the  $s$  one-electron energies were replaced by a free-electron band with a minimum at  $\epsilon_{r_1}$  (determined by the WS condition) and filled to accommodate the proper number of  $s$  conduction electrons. Here we assume that exactly one  $6s$  electron is present, so that there are no  $6s-6s$  terms to be corrected in equations such as (3.4). The renormalized  $6s$  one-electron energy admittedly provides an unsatisfactory description of the band energy in the solid, but, anticipating that the  $\epsilon_{5d}$  and  $\epsilon_{6s}$  will be replaced by band energies in Sec. IV, it does not ultimately matter what we assume at this point for those contributions. If there were more than one  $s$  conduction electron per site, a real difference between the two specifications of the renormalized atom would be introduced, and the choice made in Ref. 3 would be preferable. We might note that the renormalized  $6s$  wave function is spatially rather similar to an average radial wave function characteristic of the conduction band, and it provides a quite good representation of the band elec-

tron contribution to the Coulomb and exchange potentials of the  $5d$ ,  $4f$ , and other interior shells.

<sup>14</sup>A. J. Freeman, in *Magnetism of the Rare Earth Metals*, edited by R. J. Elliott (unpublished).

<sup>15</sup>C. Jackson, *Phys. Rev.* **178**, 949 (1969).

<sup>16</sup>N. E. Christensen and B. O. Seraphin, *Solid State Commun.* **8**, 1221 (1970); N. E. Christensen, Physics Laboratory I, Technical University of Denmark, Lyngby, Report No. 75, 1970 (unpublished).

<sup>17</sup>In Freeman's results (Ref. 14), for example, the  $d$  bandwidth is 0.35 Ry and  $\epsilon_F$  lies 0.04 Ry above the  $d$ -band minimum, so that  $\alpha$  is 0.11. Using this number together with our computed values  $\epsilon$  ( $d$  top) = +0.10 Ry,  $\epsilon$  ( $d$  bottom)

= -0.32 Ry for Eu, we place  $\epsilon_F$  at -0.27 Ry in our calculation through use of Eq. (4.1).  $\alpha$  is in all cases roughly the fraction of  $5d$  electrons present, which is consistent with the occupation of a  $d$  band having a constant density of states and a maximum occupancy of 10 electrons.

<sup>18</sup>E.g., L. Hedin and S. Lundqvist, *Solid State Physics*, Vol. 23, edited by D. Seitz, F. Turnbull, and H. Ehrenreich (Academic, New York, 1969), and references therein.

<sup>19</sup>A. P. Cracknell, *Advan. Phys.* **20**, 1 (1971), and references therein.

## Brillouin Scattering from a Microwave-Phonon Bottleneck in $\text{MgO}:\text{Ni}^{2+}$

W. J. Brya,\* S. Geschwind, and G. E. Devlin

*Bell Laboratories, Murray Hill, New Jersey 07974*

(Received 21 April 1972)

A large nonequilibrium distribution of microwave phonons arising from a phonon bottleneck has been observed in Ni-doped MgO using Brillouin light scattering; light scattering allows one to look *directly* at the phonons in a highly selective manner, and the intensity of the scattered light provides a direct measure of the effective temperatures of the phonons. With cw microwave saturation at 25.6 GHz of the  $\Delta m_s = 1$  spin transitions of the  $\text{Ni}^{2+}$  ion ( $S=1$ ) at an ambient temperature of 2°K, the effective temperatures of slow-transverse acoustic phonons at 25.6 GHz propagating near a [110] crystal direction are increased to 270–4000°K, while the bulk of the lattice modes remain at the ambient temperature; the observed phonon heatings are in reasonable agreement with theoretical predictions based on a simple rate-equation formalism applied to the  $S=1$  system. The measured bandwidth for the heated phonons is  $\sim 180$  MHz, which is significantly less than the spin resonance (EPR) linewidth of  $\sim 500$  MHz but in qualitative agreement with theory. After switching off the saturating microwaves, the phonon heating decays away in a characteristic nonlinear manner; the initial rapid drop in phonon excitation indicates an effective phonon lifetime  $\sim 5$   $\mu\text{sec}$  which is not intrinsic but determined by crystal geometry and surface condition. In accord with this relatively long lifetime, the excess phonon heating is observed to persist to ambient temperatures as high as 40°K. Under microwave saturation of the  $\Delta m_s = 1$  transitions at frequency  $\nu$ , significant heating of longitudinal phonons at  $\nu$  and  $2\nu$  has also been observed. The heating of the "forbidden" longitudinal phonons at  $\nu$  is ascribed to mode conversion of other heated  $\nu$  phonons into the longitudinal phonons at crystal boundaries, while the  $2\nu$  phonon heating arises from  $\Delta m_s = 2$  transitions in the  $S=1$  spin system. In addition, anomalously large heating (up to 40 000°K) of the slow-transverse phonons at  $\nu$  has been observed in certain spatial regions of the crystals and is tentatively ascribed to a parametric process involving the  $2\nu$  phonons.

### I. INTRODUCTION

In the usual description of the direct phonon process for spin-lattice relaxation, it is generally assumed that spins excited by resonant microwave radiation relax to phonons which are in such good contact with a thermal reservoir of infinite heat capacity (e.g., liquid helium) that the phonon excitation remains essentially at its thermal-equilibrium value. Van Vleck<sup>1</sup> pointed out many years ago, however, that the number of lattice modes on speaking terms with the spin system is actually quite limited. Consequently, if the spin-phonon coupling is strong and the thermalizing process for the phonons is slow, phonons generated over a

frequency interval comparable to the EPR linewidth will be excited above their equilibrium value. This situation, now commonly known as a phonon bottleneck, modifies the observed spin-lattice relaxation time  $T_1$  from that to be observed under the usual nonbottlenecked conditions and the relaxation is largely governed by the rate at which excess phonons can be dissipated.

Various experimental techniques have been employed to demonstrate the existence of the bottleneck. The usual spin-lattice relaxation-time measurements have disclosed unusual temperature dependences,<sup>2</sup> e.g.,  $T_1 \sim 1/T^2$  rather than  $1/T$  as for the normal direct process, sample size and concentration dependences to  $T_1$ ,<sup>2,3</sup> and nonexponential